

Mind the domain gap: Measuring the domain gap between real-world and synthetic point clouds for automated driving development

Nguyen Duc · Yan-Ling Lai · Patrick Madlindl · Xinyuan Zhu ·
Benedikt Schwab · Olaf Wysocki · Ludwig Hoegner · Thomas H. Kolbe

Received: date / Accepted: date

Abstract Owing to the typical long-tail data distribution issues, simulating domain-gap-free synthetic data is crucial in robotics, photogrammetry, and computer vision research. The fundamental challenge pertains to credibly measuring the difference between real and simulated data. Such a measure is vital for safety-critical applications, such as automated driving, where out-of-domain samples may impact a car's perception and cause fatal accidents. Previous work has commonly focused on simulating data on one scene and analyzing performance on a different, real-world scene, hampering the disjoint analysis of domain gap coming from networks' deficiencies, class definitions, and object representation. In this paper, we propose a novel approach to measuring the domain gap between the real world sensor observations and simulated data representing the same location, enabling comprehensive domain gap analysis. To measure such a domain gap, we introduce a novel metric *DoGSS-PCL* and evaluation assessing the geometric and semantic quality of the simulated point cloud. Our experiments corroborate that the introduced

N. Duc · Y. Lai · P. Madlindl · X. Zhu
TUM School of Computation, Information and Technology,
Technical University of Munich, 80333 Munich, Germany

B. Schwab · T.H. Kolbe
Chair of Geoinformatics, Technical University of Munich,
80333 Munich, Germany
e-mail: benedikt.schwab@tum.de

O. Wysocki
Chair of Photogrammetry and Remote Sensing, Technical
University of Munich, 80333 Munich, Germany
e-mail: olaf.wysocki@tum.de

L. Hoegner
Department of Geoinformatics, University of Applied Science
Munich, 80333 Munich, Germany

approach can be used to measure the domain gap. The tests also reveal that synthetic semantic point clouds may be used for training deep neural networks, maintaining the performance at the 50/50 real-to-synthetic ratio. We strongly believe that this work will facilitate research on credible data simulation and allow for at-scale deployment in automated driving testing and digital twinning.

Keywords Domain Gap · 3D Semantic Segmentation · Synthetic Point Cloud · CityGML · OpenDRIVE · CARLA Driving Simulation · Point Cloud Simulation · LoD3 Building Models

1 Introduction

The scarcity of annotated 3D point cloud data poses a challenge in training robust models for various downstream tasks, such as urban semantic segmentation, object recognition, and 3D semantic reconstruction (Li et al. 2020; Hu et al. 2021; Chen et al. 2022; Wysocki et al. 2023). It is especially apparent in the automated driving domain, where small data subsets are frequently used to verify the method's reliability, followed by the application on a broader scale. To address the problem of data scarcity, researchers have considered various approaches, such as weakly-supervised (Lin et al. 2022; Wang et al. 2024) or self-supervised (Zeng et al. 2024; Zhang et al. 2021) point cloud understanding.

However, such approaches necessitate large validation datasets for development and testing, and their performance is still limited, e.g., reaching up to around 60% accuracy for object detection (Zeng et al. 2024). An alternative, simulator-oriented approach focuses on utilizing Light Detection and Ranging (LiDAR) simulations leveraging virtual 3D environments for generating

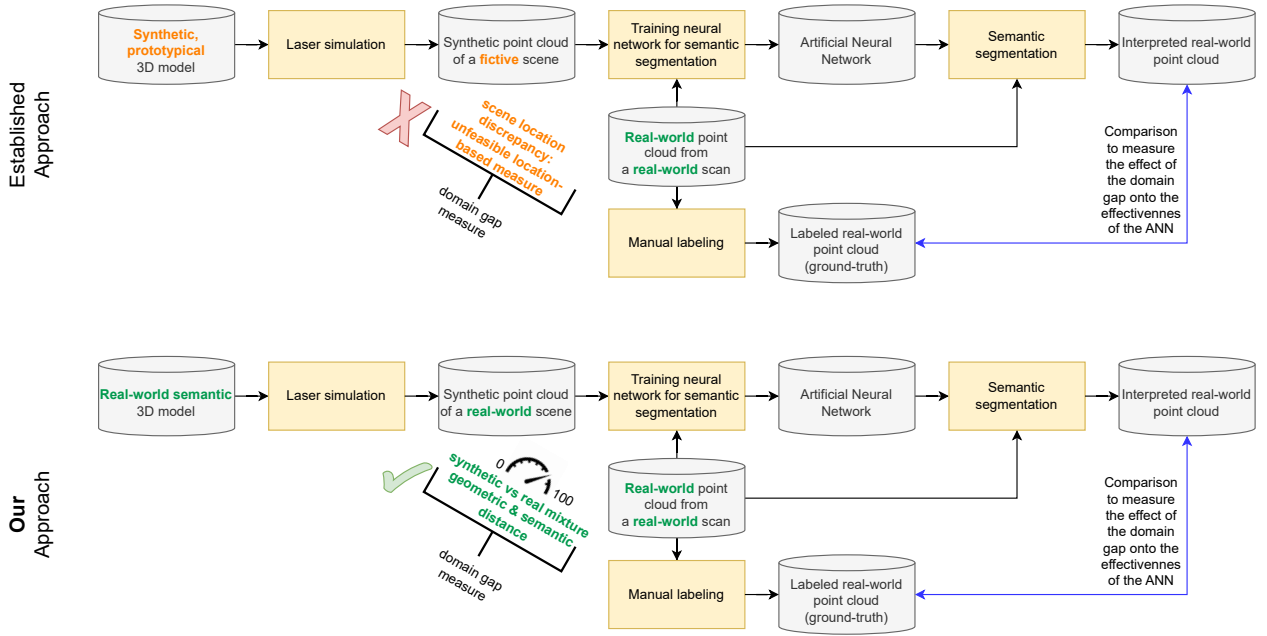


Fig. 1 Unlike the established approaches measuring the domain gap on fictive 3D models and different, real-world locations (top branch); we propose leveraging 3D models representing real-world cities and corresponding real-world point clouds for this purpose offering scene-homogeneous geometric and semantic domain gap measure (bottom branch).

an arbitrary number of data samples with various distributions aiming at mitigating the long-tail class distribution issues (Deschaud et al. 2021; Qian et al. 2024). While simulators have witnessed notable advancements recently, a significant domain gap persists between synthetic and real-world data (Stocco et al. 2023).

The term *domain gap* frequently refers to the deviation between real-world and synthetic data, as one is collected from physical and the other from digital objects. The smaller this domain gap is, the larger the potential of synthetically generated data to serve as an alternative to real-world data (Qian et al. 2024; Stocco et al. 2023). For example, the Paris-CARLA-3D dataset proposes mixing real and synthetic data for a more comprehensive class distribution (Deschaud et al. 2021). This notion raises the questions: a) How does one determine that a simulated synthetic point cloud is closer to its real-world counterpart than another? b) To what extent can simulated data replace the real counterpart in real-world scenarios?

As we show in Figure 1, the domain gap is typically measured by simulating sensor observations in a generated virtual 3D scene, then applying such synthetic data to real-world data and testing the performance discrepancy. However, this approach has several shortcomings: a) The virtual 3D scene is limited to a fictive scene created by a 3D designer and often procedural methods, not covering the complexity and perturbations of the real world; b) Also, the class description

in simulated and real data is frequently heterogeneous, impacting the validation analysis; c) Ultimately, such an approach compounds sensor noise, virtual environment imperfections, and neural networks model's performance evaluation under one metric, hampering the comprehensive analysis of real versus simulated data gap.

In this work, we are the first to introduce a method to analyze the impact of synthetic data impact on real-world scenarios by a) Deploying an actual 3D model of the real urban layout, effectively elevating discrepancies coming from the fictive model; b) introducing harmonized classes between international modelling standards and target segmentation objectives; c) effectively, allowing to analyze the domain gap without compounding factors of fictive 3D models and heterogeneous training and validation classes, enabling comprehensive geometric and semantic analysis. Moreover, we provide a framework for assessing the extent of complementary information gain stemming from simulated data to replace the costly real-world manual ground truth annotations.

Our contributions are summarized as follows:

- Introducing a harmonized class list for real-world and simulated point clouds based on the international standards OGC CityGML 2.0 and ASAM OpenDRIVE

- Developing a pipeline to simulate LiDAR sensors while preserving the semantic information according to the introduced point cloud class list
- Proposing a novel metric named *DoGSS-PCL* that measures the semantic and geometric quality of the synthetic point cloud
- Presenting a deterministic approach to evaluate the semantic and geometric domain gap of synthetic point clouds by applying the proposed metric
- Complementary analyses with a stochastic approach that measures the domain gap by comparing the performance of semantic segmentation neural networks on real-world and synthetic point clouds

2 Related Work

2.1 Driving Simulation and LiDAR Sensor Models

When developing and testing automated driving systems, submicroscopic driving simulators are utilized to simulate the vehicle's environment and its sensors. Established driving simulators include IPG CarMaker (IPG Automotive 2024), Vires VTD (von Neumann-Cosel 2014), Vector DYNA4 (Vector Informatik 2024), and the open-source solution CARLA (Dosovitskiy et al. 2017), which is based on the Unreal Game Engine. These driving simulators have interfaces to the automated driving systems under test and are real-time capable. A wide range of LiDAR sensor models exists, which differ in terms of their modeling approach, sensor effects, and validation approach (Haider et al. 2022; Hanke et al. 2017; Rosenberger et al. 2020; Zhao et al. 2021b). In order to obtain point clouds as output, ray-tracing algorithms are commonly utilized to model the propagation of the laser beams in the virtual environment model. For example, the LiDAR sensor model supplied with the CARLA driving simulator also includes effects such as signal attenuation, drop-offs in the number of points, and loss due to external perturbations.

In addition to the sensor models for automated driving, there are also LiDAR simulators, which stem from the remote sensing domain. For example, HE-LIOS++ is a simulation framework to carry out virtual laser scanning campaigns for terrestrial, mobile, Unmanned Aerial Vehicle (UAV), and airborne laser scanning (ALS) settings (Winiwarter et al. 2022). It supports the generation of full waveform data by sampling sub-rays inside the laser beam cone. To model the interaction with matter, the material properties diffuse and specular scattering coefficients, as well as the reflectance for the object surfaces, are utilized, and the ray's reflected energy is computed with the bidirectional reflection distribution function according to

Phong (Winiwarter et al. 2022; Phong 1975; Jutzi and Gross 2009).

2.2 Semantic Modeling of the Urban Environment

Most driving simulators support the import and export of OpenDRIVE-compliant road networks. OpenDRIVE is a standard for describing the lane-level road networks for developing and validating advanced driver assistance systems as well as automated driving functions. The standard is developed by the Association for Standardization of Automation and Measuring Systems (ASAM) and the current version, 1.8.0, was released in 2023 (ASAM 2023). OpenDRIVE utilizes a linear referencing concept whereby all road objects are defined relative to the reference line of the respective road. OpenDRIVE's data model is limited to representing road objects with rather abstract geometries. For example, poles, trees, and traffic signals are commonly represented by an oriented 3D bounding box or cylinder geometry. Road objects, such as buildings, controller boxes, and traffic islands, are typically represented by extruded polygonal outlines. Such abstract geometric representations of road objects are sufficient for the execution of ground-truth, geometric, and stochastic sensor models (Magosi et al. 2022). However, phenomenological and physics-based sensor models require a comprehensive and gapless representation of the road spaces (Schwab and Kolbe 2019). For such applications, the scene editors for driving simulators replace the coarse road object geometries with more detailed 3D assets and then export the graphical model alongside the OpenDRIVE dataset.

In order to represent, store, and exchange semantic models of entire cities for a broad spectrum of applications in 3D, the CityGML standard has become internationally established (Kolbe et al. 2021; Biljecki et al. 2015; Wysocki et al. 2024). The standard is issued by the Open Geospatial Consortium (OGC) and defines a conceptual data model as well as an encoding for the Geographic Markup Language (GML) (Kutzner et al. 2023). A city is hierarchically decomposed into its constituents and the city objects are modeled with respect to their geometric, semantic, and topological aspects as well as their appearance. While buildings were primarily represented in CityGML on the basis of cadastral information in the past, the focus is currently expanding to encompass the semantic representation of road spaces. CityGML supports multiple Level of Details (LODs), whereby building models in LOD2 include generalized wall surfaces with roof shapes, and starting from LOD3 the façades also encompass semantically differentiated windows, doors, and balconies.

2.3 Transfer Learning on Point Cloud Data

Traditional machine and deep learning methods require a large amount of training data, which is expensive to collect. Especially in the context of semantic segmentation of 3D point clouds, the scarcity of well-annotated data for each sensor type has become a notable challenge (Gao et al. 2022; Stocco et al. 2023; Xiao et al. 2022). The immediate application of a model trained on one sensor type to another is often infeasible owing to the different laser scanning patterns, point distribution, and point cloud size. For instance, Shen et al. (2023) show semantic segmentation decreases its performance significantly when trained on terrestrial laser scanning (TLS) and inferred on mobile laser scanning (MLS) point cloud, i.e., 76.5% to 32.0% in their experiments. Recent research endeavors have shifted towards integrating transfer learning techniques accounting for the sensor differences and showing promising results (Xiao et al. 2022), e.g., improving the results by up to 13% in segmentation accuracy in the experiments of Shen et al. (2023).

Yet, unlike in image-based transfer learning (Ros et al. 2016), there is a lack of large real-world point clouds to train a generic classifier that can be adapted for multiple scenarios (Wysocki et al. 2022). Consequently, recent years have witnessed a surge in methods investigating the adoption of synthetic point clouds complementing real-world scenarios (Wu et al. 2023; Xiao et al. 2022; Deschaud et al. 2021). However, it poses yet another challenge of not only accounting for the sensor type differences but also the domain gap between the simulated and real-world data. As reflected by experiments conducted by Xiao et al. (2022), the performance for combining simulated and real data can oscillate in the range of 55-65% accuracy depending on the scenario and benchmark dataset, underscoring the importance of further domain-gap investigations.

Although recently researchers have shown that weakly-supervised (Lin et al. 2022; Wang et al. 2024) and self-supervised (Zeng et al. 2024; Zhang et al. 2021) methods show promising results, there are still necessitating validation sets and their performance can be limited, e.g., can reach only up to 60% when deployed for object detection, as shown in the review of (Zeng et al. 2024).

Another issue impacting transfer learning is the so-called negative transfer, which, according to (Wang et al. 2019) is formulated as *transferring knowledge from the source can have a negative impact on the target learner*. One of the key issues pertains to analyzing the negative transfer not according to the algorithm but only to the target data; in the case of synthetic data,

following the standard way of training on synthetic and testing on real data (target). Another issue relates to disjoint distributions of two datasets. When labeled target data is limited, leveraging only marginal similarities is challenging, but with sufficient labeled data, a well-designed algorithm can minimize negative transfer by effectively aligning source and target distributions (Wang et al. 2019; Ge et al. 2014).

2.4 Domain Gap between Synthetic and Real-World Point Cloud

In recent years, different efforts to evaluate the domain gap for point cloud data have been undertaken (Deschaud et al. 2021; Richa et al. 2022; Huch et al. 2023). As point cloud semantic segmentation is one of the fundamental challenges, the domain gap is frequently investigated by comparing the simulated to real-world data segmentation performance (Xiao et al. 2022). The typical techniques range from domain adaptation, domain randomization, transfer learning, feature space alignment, generative methods, and hybrid training (Xiao et al. 2022; Huch et al. 2023; Guan and Liu 2021).

Simultaneously, the virtual testbed fidelity is regarded as crucial for simulating point clouds reflecting reality (Yue et al. 2018). For instance, Deschaud et al. (2021) have shown a method to create synthetic data based on computer-aided design (CAD) 3D models and the CARLA simulator. They also propose a strategy for reconstructing the environment from authentic point clouds using splats (Richa et al. 2022), aiming to create imperfect synthetic scans that resemble real-world point clouds. Still, however, the difference in semantic segmentation performance is significant; when trained on the well-established KPConv (Thomas et al. 2019), the accuracy drops by up to 38% on their Paris-CARLA-3D dataset when compared to the real data segmentation performance (Deschaud et al. 2021).

One of the flaws of such virtual worlds is that they do not represent any actual city but rather an imaginative city scene created by a 3D designer (Dosovitskiy et al. 2017). Also, CAD-generated scenes have only limited semantic information, which hinders its immediate extraction for training deep learning models, in contrast to CityGML-based models describing hierarchical semantics of each surface of a 3D model (Kolbe and Donaubauer 2021).

To the best of our knowledge, no publication investigates both the semantic and geometric simulated point cloud quality deterministically and stochastically using semantic 3D city models representing actual cities.

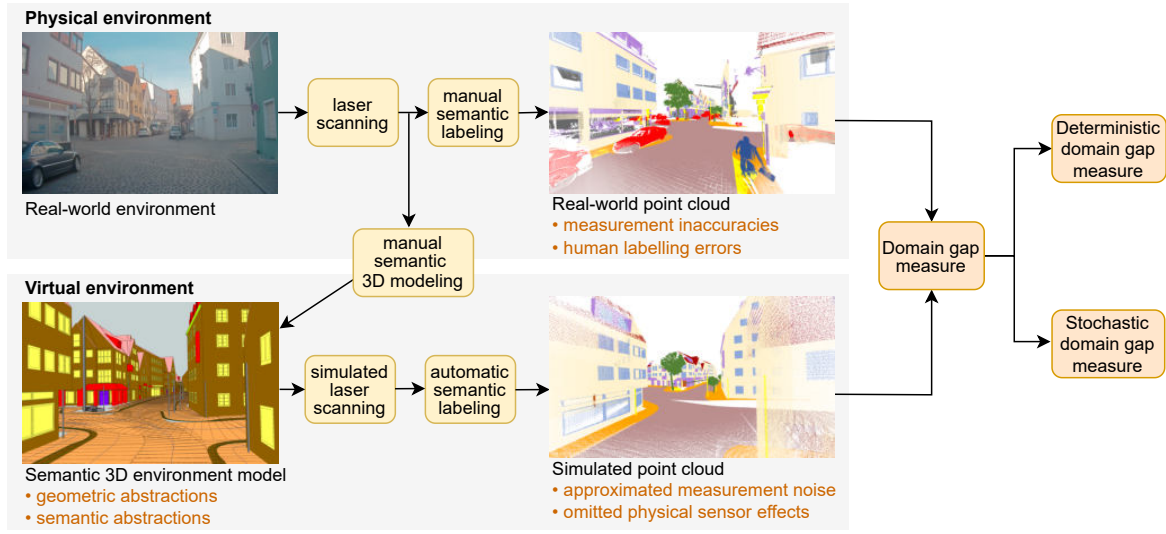


Fig. 2 Overview of our domain gap measure workflow. We leverage the real-world point clouds and manually created semantic 3D urban models to identify deterministically (Section 3.4.1) and stochastically (Section 3.4.2) the point clouds domain gap. We also propose unified semantic labels for both 3D-model-simulated and real-world point clouds in accordance with international 3D modeling standards (Section 3.1).

3 Methodology

As shown in Figure 2, we utilize real-world and synthetic point clouds simulated in the corresponding semantic 3D environment model to evaluate the domain gap. To achieve this, we introduce a set of semantic labels in Section 3.1 that is derived from the semantic modeling standards and is consistently applied to both the real-world and the synthetic point clouds. To systematically evaluate the domain gap, we introduce a deterministic approach in Section 3.4.1 and a stochastic approach in Section 3.4.2.

3.1 Semantic Point Cloud Classes

A consistent class list is required to ensure that the real-world point clouds are comparable with their simulated counterparts. Concerning our research objectives, the class list must fulfill the following requirements:

- The point clouds and the class list shall be tailored to train neural networks for semantic segmentation to analyze the domain gap stochastically. A typical problem that may influence the neural network's performance is data imbalance or skewed class proportions, often referred to as the long-tail distribution issue (Dai et al. 2017). Therefore, ideally, the number of objects in each class shall be approximately the same.
- While we desire the class list to be sufficiently detailed, it shall not be overly redundant. Instead, it

shall utilize a relatively limited number of classes describing all the critical object types that might be encountered in an urban environment. Therefore, we design our classes based on the internationally renowned urban modeling standards developed by researchers and practitioners, such as CityGML (Kolbe et al. 2021; Gröger et al. 2012) and OpenDRIVE (ASAM 2023), as well as related works (Wysocki et al. 2022; Matrone et al. 2020).

Regarding the requirements mentioned above, we present the description of our introduced 12 classes in Table 1. Furthermore, we present the relation of the classes to the international OpenDRIVE 1.4 and CityGML 2.0 standards in Table 2.

3.2 Harmonizing the Virtual Environment

In order to simulate a LiDAR sensor in the virtual environment and to obtain the semantic labels automatically, the semantic environment models need to be prepared accordingly for the simulator. As the domain gap is specifically investigated for the development and testing of automated driving, the submicroscopic open-source driving simulator CARLA is employed for the sensor simulation. CARLA supports the simultaneous simulation of further exteroceptive sensors, such as RADAR and camera, which are required for testing the perception system and for further potential downstream domain gap analyses. To derive an en-

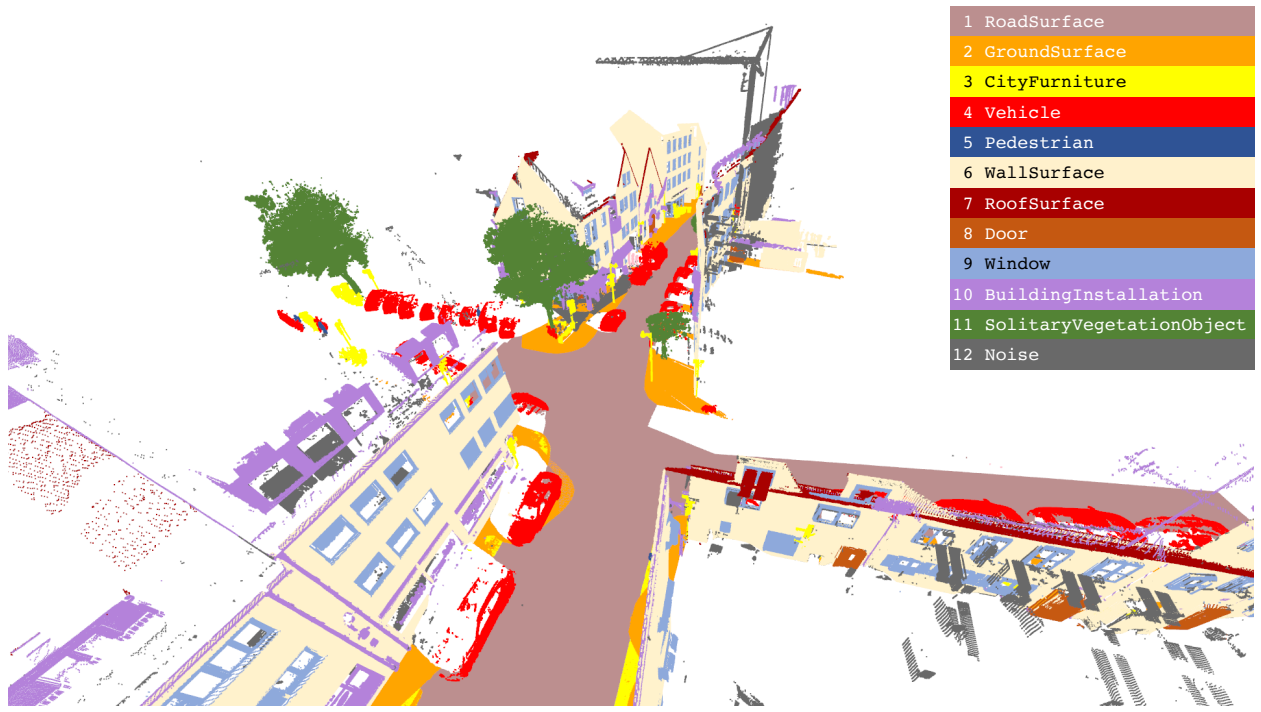


Fig. 3 Real-world point cloud, which was manually labeled according to the class list of Table 2.

vironment model representation for CARLA while preserving the relevant semantic labels of the objects, we developed a model preparation and processing chain shown in Figure 4.

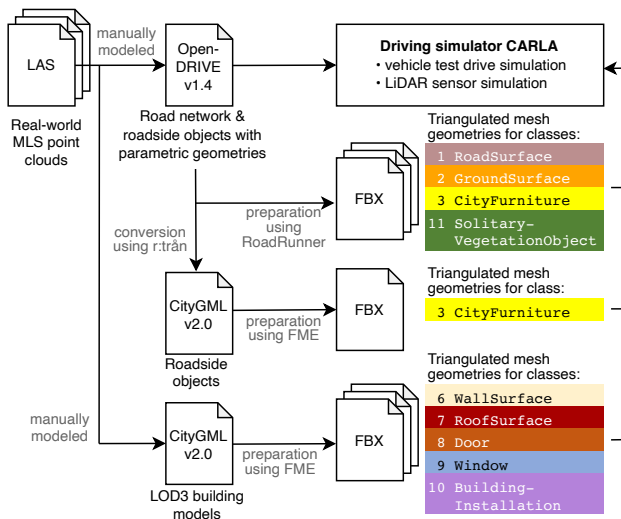


Fig. 4 Developed model processing chain that enables a LiDAR scanning simulation with automatically assigned labels according to our proposed class list. The road network standard OpenDRIVE and the semantic 3D city model standard CityGML serve as the basis for deriving application-specific mesh geometries.

CARLA imports the road network description from OpenDRIVE datasets, which enables the simulated vehicle agents to plan routes and driving trajectories at the lane level. In order to simulate the LiDAR sensor in CARLA with automatic labeling according to our proposed class list, a triangulated mesh geometry representation of the environment is required, whereby the semantic labels must be retained.

As depicted in Figure 4, we utilized three processing paths to derive triangulated mesh geometries from the semantic 3D environment models. First, we used the 3D scene editor *RoadRunner* (Mathworks 2018) to generate mesh geometry representations for the road surfaces and ground surfaces from the OpenDRIVE dataset. This also includes traffic lights and signs, which are classified under **CityFurniture**, and trees under the class **SolitaryVegetationObject**. Since *RoadRunner* does not support the full range of road objects that are represented in OpenDRIVE, we use the open-source tool *r:trān*¹ to convert the OpenDRIVE dataset to CityGML 2.0 (Schwab et al. 2020). This second path includes fence and road-boundary wall objects, whereby the geometries are triangulated and combined using the tool Feature Manipulation Engine (FME). In the third path, the LOD3 building models are utilized, which have been modeled manually on the basis of the real-world point clouds and are already available as

¹ Website: <https://rtron.io>

Table 1 Description of our introduced 12 road space classes.

ID	Class/ description
1 ■	RoadSurface Describes any vehicle-allowed surfaces, w/o sidewalks and other road installations
2 ■	GroundSurface Pedestrian-allowed surfaces, w/o roads
3 ■	CityFurniture Any vertical urban installation, w/o building-attached objects
4 ■	Vehicle Any vehicle, parked or moving
5 ■	Pedestrian Any person, standing or moving
6 ■	WallSurface Vertical and planar building parts, w/o roofs, installations, and facade elements
7 ■	RoofSurface Building parts forming roof structures
8 ■	Door Any opening allowing entering objects, w/ gates
9 ■	Window Any opening and its outer blinds, w/o entries
10 ■	BuildingInstallation Any building-attached installation
11 ■	SolitaryVegetationObject Any vegetation, w/ tree trunks and branches
12 ■	Noise Noisy points and any other non-annotated element

CityGML 2.0 datasets. Thereafter, the object geometries are also triangulated using the tool FME and the mesh geometries are stored separately according to our proposed class list.

Since the OpenDRIVE and CityGML datasets are georeferenced, the geometries were translated into a local coordinate reference system for the driving simulator. As a result, we have a simulation environment derived from the semantic 3D model that reflects the physical environment with relative accuracy in the low centimeter range, as shown in the overview Figure 2.

3.3 Simulating Laser Scanning

After importing the virtual environment into the sub-microscopic driving simulator, we set up a virtual vehicle with LiDAR sensors to collect the point cloud data. CARLA supports the configuration of the vehicle's sensor suite and environmental conditions to reproduce a driving scenario. Since the exact sensor configuration was not disclosed by the company that conducted the real-world MLS campaign, we have approximated the sensor positions and configuration parameters as closely as possible based on (3D Mapping Solutions 2023; Gräfe 2007). Figure 5 shows the simulated vehicle test drive

and the corresponding point cloud obtained from this timestamp.

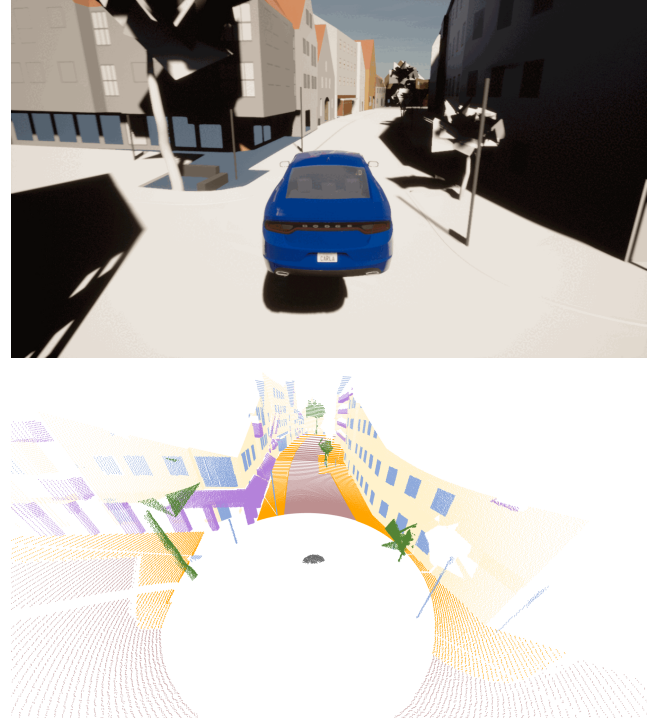


Fig. 5 Simulated test drive in the virtual environment with the automatically labeled point cloud after applying noise in the post-processing. The virtual vehicle was elevated to match the sensor positions of the real-world surveying vehicle.

As CARLA's semantic LiDAR sensor model lacks built-in noise support, we introduce noise during post-processing by applying a Gaussian distribution to the distance measurements along the raycasted vector. We assume that the distance measurement error is normally distributed with a standard deviation of $\rho = 2$ cm, following Spiegel and Chen (2021). Figure 6 shows the

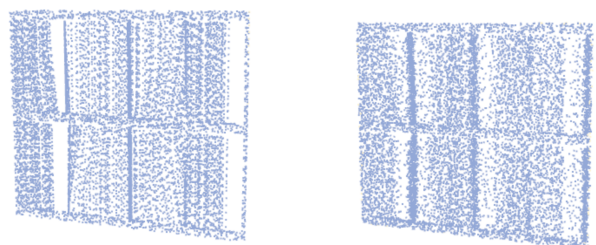


Fig. 6 Scan of a window with curtains in the interior before (left) and after (right) adding noise.

simulated point cloud of a window object with curtains

Table 2 Correspondences between the classes of OpenDRIVE 1.4 and CityGML 2.0, and their mapping to the introduced point cloud classes. The colors are used in the remaining illustrations.

Semantic 3D environment model		Point clouds (real-world and simulated)	
OpenDRIVE 1.4	CityGML 2.0	ID	Class
<code>LaneSectionLRLane</code> (type: driving)	<code>TrafficArea</code> (function: 1)	1	<code>RoadSurface</code>
<code>RoadObject</code> (type: barrier, name: raisedMedian)	<code>AuxiliaryTrafficArea</code>		
<code>RoadObject</code> (type: barrier, name: trafficIsland)	<code>AuxiliaryTrafficArea</code>		
<code>RoadObject</code> (type: roadMark)	<code>AuxiliaryTrafficArea</code>		
<code>LaneSectionLRLane</code> (type: sidewalk)	<code>TrafficArea</code> (function: 2)	2	<code>GroundSurface</code>
<code>LaneSectionLRLane</code> (type: border)	<code>AuxiliaryTrafficArea</code>		
<code>LaneSectionLRLane</code> (type: none, material: grass)	<code>AuxiliaryTrafficArea</code> <code>OuterFloorSurface</code>		
<code>Signal</code> (name: trafficLight)	<code>CityFurniture</code>	3	<code>CityFurniture</code>
<code>Signal</code> (name: traffic signs)	<code>CityFurniture</code>		
<code>RoadObject</code> (type: pole, name: streetLamp)	<code>CityFurniture</code>		
<code>RoadObject</code> (type: pole, name: trafficLight)	<code>CityFurniture</code>		
<code>RoadObject</code> (type: pole, name: trafficSign)	<code>CityFurniture</code>		
<code>RoadObject</code> (type: barrier, name: fence)	<code>CityFurniture</code>		
<code>RoadObject</code> (type: obstacle, name: controllerBox)	<code>CityFurniture</code>		
<code>RoadObject</code> (type: obstacle, name: bench)	<code>CityFurniture</code>		
<code>RoadObject</code> (type: barrier, name: wall)	<code>CityFurniture</code>		
—	—	4	<code>Vehicle</code>
—	—	5	<code>Pedestrian</code>
<code>RoadObject</code> (type: building, surf. orientation: side)	<code>WallSurface</code>	6	<code>WallSurface</code>
<code>RoadObject</code> (type: building, surf. orientation: top)	<code>RoofSurface</code>	7	<code>RoofSurface</code>
—	<code>Door</code>	8	<code>Door</code>
—	<code>Window</code>	9	<code>Window</code>
—	<code>BuildingInstallation</code>	10	<code>BuildingInstallation</code>
—	<code>OuterCeilingSurface</code>		
<code>RoadObject</code> (type: tree)	<code>SolitaryVegetationObject</code>	11	<code>SolitaryVegetationObject</code>
<code>RoadObject</code> (type: vegetation)	<code>SolitaryVegetationObject</code>		
—	—	12	<code>Noise</code>

before and after applying normal-distributed noise to the distance measurements.

3.4 Measuring Domain Gap Between Real-World Data and Synthetic Data

We propose a deterministic and stochastic approach to investigate the concept of domain gap. The deterministic approach involves computing distances and designing a custom metric named *Domain Gap of Simulated Semantic Point Cloud (DoGSS-PCL)* to quantify how well the synthetic point clouds match the real-world ones. The stochastic approach involves utilizing synthetic and real-world point clouds in a common deep-learning-based task: 3D semantic segmentation. We focus on the 3D point cloud semantic segmentation while assessing its inference performance, leveraging well-established metrics in the semantic segmentation field. Here, the real-world point cloud serves as the ground-truth dataset.

3.4.1 Deterministic Approach

To compare the real-world point cloud \mathcal{R} with the synthetic point cloud \mathcal{S} deterministically, we compute

- (1) **Semantic-Based Point Cloud Distance (SBPCD)** $d(\mathcal{R}, \mathcal{S})$ to measure between the point clouds \mathcal{R} and \mathcal{S}
- (2) **Domain Gap of Simulated Semantic Point Cloud (DoGSS-PCL Metric)** $m_{DoGSS-PCL}(\mathcal{R}, \mathcal{S})$ that allows to compare and benchmark synthetic point clouds \mathcal{S}_i given one corresponding real-world point cloud \mathcal{R} (2).

(1) Semantic-Based Point Cloud Distance We choose to compute and weigh two distance measures.

(a) First, a cloud-to-cloud distance $d_{C2C}(\mathcal{R}, \mathcal{S})$ between the two point clouds \mathcal{R}, \mathcal{S} (Girardeau-Montaut et al. 2005; Batur et al. 2020):

$$d_{C2C}(\mathcal{R}, \mathcal{S}) = \max_{a \in \mathcal{R}_p} \left\{ \min_{b \in \mathcal{S}_p} \{d(a_{\mathcal{R}}, b_{\mathcal{S}})\} \right\}, \quad (1)$$

where $a_{\mathcal{R}}$ are the points of set \mathcal{R}_p ; $b_{\mathcal{S}}$ are the points of set \mathcal{S}_p ; $d(a_{\mathcal{R}}, b_{\mathcal{S}})$ is the Euclidean distance between $a_{\mathcal{R}}$ and $b_{\mathcal{S}}$.

(b) Secondly, making use of semantic information present in the point clouds, we compute a mean class-wise M3C2 distance $d_{MM3C2}(\mathcal{R}, \mathcal{S})$ (Lague et al. 2013). Let C be the number of classes in both \mathcal{R} and \mathcal{S} . Then we split the point clouds into class-wise point clouds, such that $\mathcal{R} = \bigcup_{c=1}^C \mathcal{R}^{(c)}$ and $\mathcal{S} = \bigcup_{c=1}^C \mathcal{S}^{(c)}$. On each pair $(\mathcal{R}^{(c)}, \mathcal{S}^{(c)})$, we perform M3C2 and take the median of inlier M3C2 distances: $\tilde{\mathbf{d}}_{\mathbf{M3C2}}(\mathcal{R}^{(c)}, \mathcal{S}^{(c)})$. Outlier points, i.e., points where M3C2 has found no matches, are ignored. We then average the absolute values of the medians with custom class weights to enable balancing the importance of each class in the evaluation $\{w^{(c)}\}_{c=1}^C$ where $\sum_{c=1}^C w^{(c)} = 1$:

$$d_{MM3C2}(\mathcal{R}, \mathcal{S}) = \sum_{c=1}^C w^{(c)} \cdot \tilde{\mathbf{d}}_{\mathbf{M3C2}}(\mathcal{R}^{(c)}, \mathcal{S}^{(c)}) \quad (2)$$

The distance $d_{\mathcal{R}, \mathcal{S}}$ is a weighted mean between the absolute value of $d_{C2C}(\mathcal{R}, \mathcal{S})$ and $d_{MM3C2}(\mathcal{R}, \mathcal{S})$:

$$d(\mathcal{R}, \mathcal{S}) = \lambda_1 d_{MM3C2}(\mathcal{R}, \mathcal{S}) + \lambda_2 d_{C2C}(\mathcal{R}, \mathcal{S}) \quad (3)$$

The distance has the same physical unit as point clouds \mathcal{R} and \mathcal{S} and represents an absolute Euclidean deviation between the clouds in the world frame (L2 distance).

(2) **DoGSS-PCL Metric** We combine $d_{C2C}(\mathcal{R}, \mathcal{S})$ and $d_{MM3C2}(\mathcal{R}, \mathcal{S})$ with a semantic measure, the weighted mean intersection over union (mIoU), to form the metric $m_{\mathcal{R}}(\mathcal{S})$, while following the standard IoU formulation (analogical to Eq. 6):

$$mIoU(\mathcal{R}, \mathcal{S}) = \sum_{c=1}^C w^{(c)} \cdot IoU(\mathcal{R}^{(c)}, \mathcal{S}^{(c)}). \quad (4)$$

We normalize with the min-max normalization the result to the interval $[0, 1]$, where 0 indicates the best possible match, and 1 translates to the worst match. $mIoU(\mathcal{R}, \mathcal{S})$ behaves inversely in the sense that good values are close to 1 and poor values close to 0. We thus use an mIoU factor $f_{mIoU}(\mathcal{R}, \mathcal{S}) = \frac{1}{mIoU(\mathcal{R}, \mathcal{S}) + \varepsilon}$, where $\varepsilon > 0$ and should be chosen empirically and small to improve the numerical stability. Let the growth function be bounded by exponential upper-bound (Mohri 2018) controlled by empirically set α distance weight, defining the metric as (subtracted by one to normalize and obtain reverse score):

$$m_{\text{DoGSS-PCL}}(\mathcal{R}, \mathcal{S}) = 1 - \exp \left[\alpha(d(\mathcal{R}, \mathcal{S}) + \lambda_3 f_{mIoU}) \right] \quad (5)$$

The DoGSS-PCL metric enables measuring different synthetic point clouds $\mathcal{S}_1, \dots, \mathcal{S}_n$ and comparing their $m_{\text{DoGSS-PCL}}(\mathcal{R}, \mathcal{S})$ scores.

The $\lambda_1, \lambda_2, \lambda_3$ express weights assigned to the specific characteristic, which balance: λ_1 importance for the class-wise change; λ_2 cloud-to-cloud L2 distance; λ_3 semantic discrepancies. Let $\lambda_1 + \lambda_2 + \lambda_3 \in [0, 1]$ where $\lambda_1 + \lambda_2 + \lambda_3 = 1$ and shall follow $\lambda_1 > \lambda_2 > \lambda_3$ allowing for balanced weighting of the selected parameters and features. Also, the weights should be chosen concerning balancing distance scores and importance of $\alpha(d(\mathcal{R}, \mathcal{S}))$.

3.4.2 Stochastic Approach

While deterministic measurement quantitatively assesses the similarity between real-world and synthetic point clouds, it does not give full intricacies for the frequently sought-after downstream scene understanding tasks. One of the prominent examples of data-scarce tasks is point cloud semantic segmentation (Wysocki et al. 2023). We leverage the established deep-learning-based 3D point cloud semantic segmentation models as benchmarks and utilize the established evaluation metrics to quantify and compare the network training performance. We propose mixed setups of point clouds with different proportions of real-world and synthetic point clouds that gradually amplify the influence of synthetic point clouds on the downstream segmentation task. These setups with the same quantity but increasing proportions of synthetic point clouds manifest the trade-off between model performance and the usage of synthetic point clouds.

We evaluate the model with class-wise $IoU^{(c)}$, which intersection over union (IoU) of class c is calculated as follows:

$$IoU^{(c)} = \frac{TP^{(c)}}{TP^{(c)} + FP^{(c)} + FN^{(c)}}. \quad (6)$$

where $TP^{(c)}$, $FP^{(c)}$, and $FN^{(c)}$ stand for true positive, false positive, and false negative, respectively. We use mIoU to evaluate the learning and classification quality of the models on each training set, which is calculated by taking the average of class-wise $IoU^{(c)}$. We assess the influence of the proportion of synthetic point clouds on the class-wise $IoU^{(c)}$ performance. We evaluate the Pearson correlation coefficient between the class-wise $IoU^{(c)}$ and the synthetic point cloud proportion. Let

i be the index of the training set that consists of p_i percent of synthetic data, I be the set that contains all of the indexes of the training sets, and P be the set contains all of p_i . The index $IoU_i^{(c)}$ represents the $IoU^{(c)}$ performance of set i and IoU_c represents the set contains all of $IoU_i^{(c)}$. We calculate the correlation coefficient of class c as follows:

$$corr^{(c)} = \frac{cov(P, IoU_c)}{\sigma_P \sigma_{IoU^{(c)}}}. \quad (7)$$

where $cov(P, IoU_c)$ is the covariance between P and IoU_c calculated as follows:

$$cov(P, IoU^{(c)}) = \sum_{i \in I} (p_i - \mu_p)(IoU_i^{(c)} - \mu_{IoU^{(c)}}). \quad (8)$$

and σ_P and $\sigma_{IoU^{(c)}}$ are the standard deviations of P and $IoU^{(c)}$ calculated as follows:

$$\sigma_P = \sqrt{\sum_{i \in I} (p_i - \mu_p)^2}. \quad (9)$$

$$\sigma_{IoU^{(c)}} = \sqrt{\sum_{i \in I} (IoU_i^{(c)} - \mu_{IoU^{(c)}})^2}. \quad (10)$$

where mean of P is denoted by μ_p and of $IoU^{(c)}$ by $\mu_{IoU^{(c)}}$. The correlation coefficient is positive when the performance improves as synthetic data quality increases and is negative when the performance downgrades as synthetic data quality increases.

We employ 3D point cloud semantic segmentation networks PointNet++ (Qi et al. 2017) and KPConv (Thomas et al. 2019), both established in 3D semantic segmentation tasks and in the geospatial community, due to their reliable performances and their direct operations on unordered point clouds: Both methods support training on mere 3D points. Their architectures are designed to utilize spatial relationships between neighboring points to identify local 3D structures. While they both leverage the spatial property of the point clouds, PointNet++ extracts the geospatial feature with a set of abstraction levels and multi-layer perceptrons stacking up in a hierarchical structure, and KPConv leverages 3D kernels to aggregate local neighborhood information. An advantage of using KPConv is that it provides an effective batch selection pipeline that can directly operate on a significant number of points in a point cloud, thus eliminating the need to handcraft a split of large point cloud files into separate scenes beforehand.

4 Experiments

We compared the synthetic point cloud with its real-world counterpart to evaluate the domain gap between the two representations. The synthetic point cloud covers the same area as the real-world point cloud since it was simulated in the semantic 3D environment model. In turn, the semantic model was manually created utilizing the same real-world point cloud. The setup ensures minimum divergence between both point cloud representations in terms of temporal changes in the environment.

We evaluated the synthetic point cloud generated by our proposed approach using the stochastic and deterministic methods. We applied the evaluation methods outlined in Section 3.4 to both real-world and synthetic point clouds, analyzing the differences. In order to evaluate the domain gap with the stochastic approach, we conducted data splits to synthetic and real-world data, which are illustrated in Figure 7. The complete implementation of the experiments can be found in our repository, which is provided in the code availability statement.

4.1 Real-world data acquisition

Our real-world point cloud dataset is captured along a designated route within the Ingolstadt city center. The dataset covers an approximate area of 400 meters by 250 meters and includes detailed information on over 50 distinct constructions. The architectural styles of these buildings are commonly seen throughout Germany.

4.1.1 Mobile mapping point clouds

The MLS point cloud was acquired by 3D Mapping Solutions and their in-house mobile mapping platform, which geo-referencing was supported by the German SPOS RTK system. The platform was mounted on a mini-van and drove while collecting the data in the city center of Ingolstadt, Germany. Approximately 100M points with density up to 3000 pts/m^2 were recorded, whereby the setup ensured their relative accuracy in the range of 1-3 cm (3D Mapping Solutions 2023).

To ensure high-quality labeling with limited resources, we implemented a four-stage process. First, we employed connected-component-based geometric classification to split up the original point cloud into N subsets of point clouds, each of which contains points that are geometrically close to each other while having some distance from other groups. Secondly, we performed ground segmentation to differentiate the ground

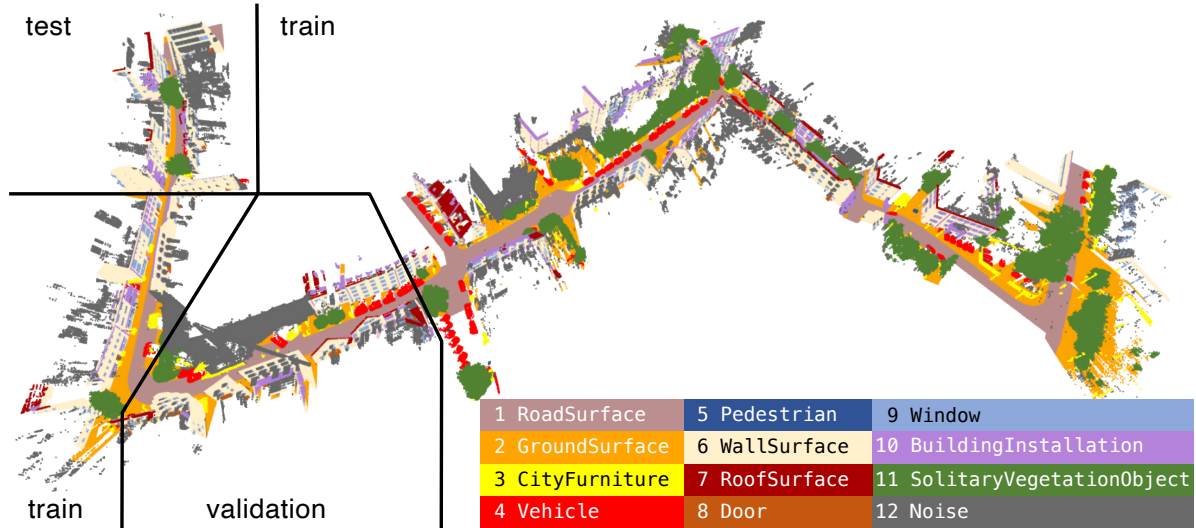


Fig. 7 Data split of real-world point clouds with street lengths of approx. 510 meters for training, 77 meters for validation, and 85 meters for testing.

planes, such as roads, pavements, and soil from 3D objects with height. This step yielded a significant increase in accuracy due to the prior removal of separable objects and noise points. Next, we manually labeled the point clouds employing a polyline segmentation tool and assigned each point cloud to a numerical value corresponding to the defined classes in Section 3.1. Finally, we merged all labeled subsets and resolved duplicates into one point cloud dataset.

4.1.2 Semantic 3D city model

For our experiments, we acquired the semantic 3D city model comprising of LOD3 buildings and the road environment representing the city center of Ingolstadt in Germany.² Figure 8 lists the number of objects per class of our semantic environment model in CityGML. These models served as inputs for our synthetic data generation after applying our method described in Section 3.2. Notably, these models were created manually based on the MLS point cloud described in the previous Section 4.1.1, thus avoiding discrepancies caused by different point clouds obtained in different epochs. In our experiments, we used version 0.9.14 of the sub-microscopic driving simulator CARLA as our simulation testbed, which is based on the Unreal Engine version 4 (Epic Games 2019).

Even though we have acquired highly detailed 3D city models, some objects only approximated the real-world representation. For example, our pipeline did not use specific methods to process complex meshes, such as

trees and bushes, and thus, these elements lack geometric accuracy. Despite the comprehensive LOD3 models, very fine geometric structures of the real world are still generalized, such as the surface structure of doors or facade decorations.

4.2 Synthetic Semantic Point Cloud

To validate our method, we set up a synthetic data generation pipeline in our experiment utilizing the methodology presented in Section 3.2 and created a synthetic dataset with 100M points, which yields approximately the same ratio as our real-world point cloud. The distribution of the synthetic points compared to the real-world points per class and dataset split is depicted in Figure 9.

Since the ground-truth vehicle trajectory is not disclosed by the surveying company along with the real-world point cloud, we approximated a plausible ego-vehicle trajectory. To avoid robotic driving behavior, we designed the control of the ego vehicle as a video game setup and drove manually. The simulated LiDAR mimicked real-world sensors, capturing scans at realistic rates with post-processing as mentioned in Section 3.3. The physical interactions between artifacts, such as collision and gravitational forces, were deactivated due to unexpected behavior from vehicle-obstacle interactions. Figure 10 illustrates the real-world point cloud of a street section side-by-side with the synthetically generated counterpart. Around 100M points were generated for the entire area, which is comparable to the acquired real point cloud. As we mentioned in Section 4.1.2, some 3D objects approximated the real-world

² The OpenDRIVE and CityGML datasets used for the experiments are available under <https://github.com/savenow/lod3-road-space-models>

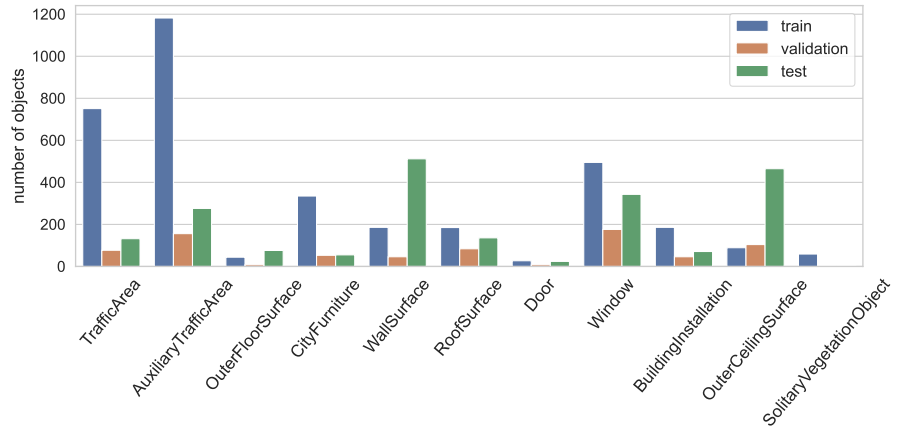


Fig. 8 Number of object instances per class in the train, test, and validation CityGML dataset.

point cloud representation. This phenomenon is shown in Figure 11.

4.3 Evaluation of the Deterministic Approach

4.3.1 Parameters

Since our real-world point clouds are georeferenced, we first translated them into the same local reference frame as the synthetic point cloud. We calculated the mIoU utilizing a voxel structure and chose a voxel size of $l_{voxel} = 0.5$ m, following the usual divergence in the geo-registration of mobile mapping point clouds (Zhu et al. 2020; Wysocki et al. 2023). The voxel size was chosen empirically considering point cloud density and experiments performed under arbitrary translation values listed in Table 3.

Table 3 Metric sensitivity with the selected offset distances under constant voxel size in the local reference frame.

	Offset		
	0.0 m	0.1 m	0.3 m
$m_{DoGSS-PCL}(\mathcal{R}, \mathcal{S})$	0.09	0.51	0.59
$d(\mathcal{R}, \mathcal{S})$	0.15	0.46	0.55
d_{MM3C2}	0.04	0.22	0.35
d_{C2C}	0.31	0.80	0.85
$mIoU$	29.07%	3.10%	2.50%

The class weights for mIoU and d_{MM3C2} were chosen to emphasize building-related classes and are shown in Table 4. We considered walls essential as they constitute the primary geometry of buildings and, thus, the city's geometry. We decided to perform the comparison on well-represented static objects, as listed in

Table 4. In consequence, the comparison omits the dynamic objects not present in the virtual model, such as **Vehicle**, **Pedestrian**; also, largely simplified objects, such as **RoadSurface**, **SolitaryVegetationObject**; as well as noise represented by the **Noise** class. For the

Table 4 Weights per class used for weighted average computation mIoU and d_{MM3C2} , chosen based on the heuristic and class importance.

Class	Weight
CityFurniture	0.1
GroundSurface	0.1
WallSurface	0.2
RoofSurface	0.15
Door	0.15
Window	0.15
BuildingInstallation	0.15

metric $m_{\mathcal{R}}(\mathcal{S})$, we chose the weights and consider that by construction, even acceptable mIoU values will lead to high scores. To have a balance between d_{MM3C2} and f_{mIoU} , we thus empirically selected $\lambda_1 = 0.6$, $\lambda_2 = 0.3$, and $\lambda_3 = 0.1$ for f_{mIoU} . For the bounded growth rate, we empirically chose $\alpha = -0.2$ as it led to a wide range of values in the range $[0, 1]$ being used with the data for this paper.

As the metric proposed indicates only the relative fit of the synthetic point clouds, the parameters for the metric can be freely tuned by the user as long as they remain constant for all synthetic point clouds that are compared at a time.

4.3.2 Results

To better demonstrate the sensitivity of our deterministic approach, we randomly translated the synthetic

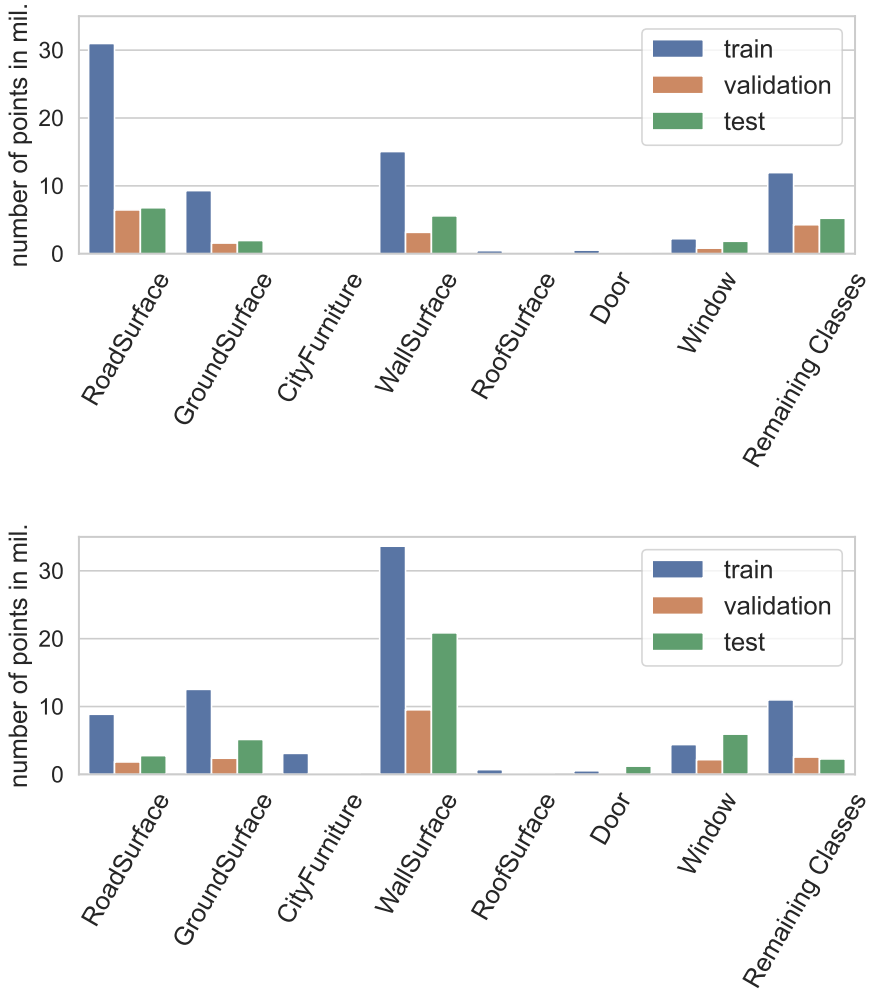


Fig. 9 Number of points per object class for real-world (left) and synthetic data (right).



Fig. 10 Comparison of the real-world (left) and synthetic point clouds (right) highlighting the discrepancies due to abstractions in the environment and sensor model.

point cloud by around 1 m and evaluated our DoGSS-PCL metric on both the original and translated versions. The results are presented in Table 5.

With the synthetic point cloud \mathcal{S} , the distances were in a cm range, while the mIoU was in a low two-digit span. This led to a relatively small $IoU^{(c)}$ factor of 3.44. Accordingly, the original synthetic point cloud

performed well on our custom metric with a value of $m_{DoGSS-PCL}(\mathcal{R}, \mathcal{S}) = 0.09$, which was much closer to 0 than to 1 and thus constituted a good value given the metric parameters we chose.

For the translated synthetic point cloud, the mIoU score decreased by one order of magnitude. This decrease was influenced by the voxel size $l_{voxel} = 0.5$ m <



Fig. 11 Synthetic point cloud of a tree in green and its real-world counterpart in gray. The synthetic point cloud representation contains all the elements of a tree, such as branches and leaves, but the geometric shapes are different.

Table 5 Distance and metric results.

	Synthetic	Synthetic (translated)
$m_{DoGSS-PCL}(\mathcal{R}, \mathcal{S})$	0.09	0.73
$d(\mathcal{R}, \mathcal{S})$	0.15	1.14
d_{MM3C2}	0.04	1.01
d_{C2C}	0.31	1.34
$mIoU$	0.29	0.02
f_{mIoU}	3.44	54.79

$1.14 = d(\mathcal{R}, \mathcal{S})$ being smaller than the cloud distance. Essentially, the resolution of the $IoU^{(c)}$ calculation was higher than the distance of points, which led to low $IoU^{(c)}$ scores. In contrast, with the non-translated synthetic point cloud $d(\mathcal{R}, \mathcal{S}) = 0.15 < 0.5 = l_{voxel}$, thus the $IoU^{(c)}$ was significantly higher. The low $mIoU$ as well as the higher distances led to a metric score of $m_{DoGSS-PCL}(\mathcal{R}, \mathcal{S}) = 0.73$, which was closer to 1 than to 0 and much higher than the translated score of $m_{DoGSS-PCL}(\mathcal{R}, \mathcal{S}) = 0.09$.

4.4 Evaluation of the Stochastic Approach

4.4.1 Parameters

We designed the following training sets of the real-to-synthetic ratio: 100%-0%, 75%-25%, 50%-50%, 25%-75%, and 0%-100%. The former percentage indicates the quantity ratio of the real-world point cloud to the

set, and the latter is the quantity ratio of the synthetic point cloud to the set. For each set, we randomly sourced points from the real-world domain and synthetic domain, respectively, to the desired proportions, then concatenated both point clouds into a single point cloud. We used the training split area specified in Figure 7 to establish the training sets. We evaluated the results on the test split of the real-world point clouds. Figure 12 visualizes the result for a 50%-50% mixture of real-world (Figure 12a, blue color palette) and synthetic data (Figure 12b, red color palette). Figure 12c shows the case where the synthetic point cloud complemented a region of the wall surface that was occluded by the tree.

To train PointNet++ with our datasets, we split our point clouds into sub-scenes. In each iteration, an input scene served as a batch and passed through the model. Since KPConv randomly samples input batches directly from large point clouds, it eliminated the need to split the point clouds into small scenes beforehand. In each iteration, several points and their spherical neighborhoods were queried, augmented, and stacked together as an input batch. To sample different regions of the clouds more evenly, selected points in an iteration were made to be chosen less likely in the subsequent iterations.

We trained both networks with point coordinates without additional features such as color or normal vectors. The model structures, optimizers, losses, and hyperparameters, such as the neighborhood querying radius of PointNet++ and KPConv, were inspired by and followed the ones used in the original works. The models were evaluated on the unseen test real-world point cloud data, as shown in Table 6, Table 7, and in Figure 13.

4.4.2 Results

We observe that KPConv outperforms PointNet++, corroborating the current research consensus, e.g., as reported in the Paris-Carla-3D dataset (Deschaud et al. 2021).

The performance difference between the two models is substantial, as found in Table 6 and Table 7. Hence, when analyzing the domain gap between synthetic and real-world data, we focused mainly on the results of KPConv as it provided us with a much more comprehensive evaluation than the results of PointNet++.

In general, the $mIoU$ decreases as the ratio of synthetic data increases with $corr. = -0.8$ for KPConv and $corr. = -0.62$ for PointNet++. Nevertheless, with 50% of synthetic data, KPConv still performs close to the results of training KPConv with 100% real-world

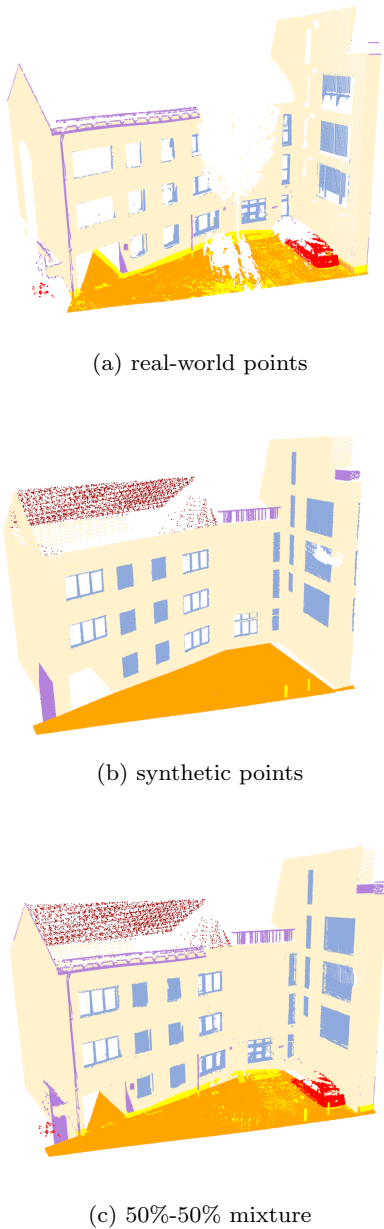


Fig. 12 Real-world and synthetic point cloud mixture.

data. Generally, the performance worsens as the ratio of synthetic point clouds increases. An exception is the **RoofSurface** class, which holds a positive correlation coefficient of 0.60 with KPCConv and 0.12 with PointNet++. Unlike the other classes, the $IoU^{(c)}$ of **RoofSurface** object class increases as the synthetic point clouds increase.

We provide the class-wise $IoU^{(c)}$, mIoU, and the correlation coefficient results in Table 6, Table 7, and in Figure 13.

5 Discussion

5.1 Deterministic Approach

The *DoGSS-PCL* metric we propose evaluates the quality of synthetic point clouds by combining physical and semantic distances into a single score *DoGSS-PCL* $\in [0, 1]$. By capturing both global and semantic grouped distance, the metrics can capture both global changes and semantic mismatches. We showcase its effectiveness by comparing well-fitting semantic point clouds with translated ones (Table 5). As expected, the well-fitting version achieves a significantly lower *DoGSS-PCL* score, highlighting its capturing capabilities of both global structure and semantic fidelity. Notably, *DoGSS-PCL* provides a versatile evaluation, measuring global and semantic-based geometric mismatch, while also incorporating f_mIoU to assess semantic accuracy, particularly for underrepresented classes.

The synthetic point cloud is well aligned geometrically and harmonized semantically, which could be seen from our metric *DoGSS-PCL*. In detail, the recorded global mismatch is quite small with mean bi-directional $d_{C2C} \approx 0.1$. The distance becomes even smaller when we consider semantic information, where most classes maintain a small stable deviation between real-world and synthetic point clouds with a mean of 0.04 and a standard deviation around 0.5. d_{MMC2C} can also capture the difference in geometry of the **RoofSurface**, **GroundSurface**, and **BuildingInstallation**. However, this would only be reflected by an increase of the mean distance to 0.08 and standard derivation to 0.14. Unfortunately, these increases would make a minor contribution to our final result due to the imbalance in the number of points.

While metrics such as d_{C2C} and d_{MMC2C} effectively capture the overall discrepancy between two point clouds, they fail to account for subtle variations in geometric characteristics. These geometric details are critical when comparing synthetic and real-world point clouds, as even minor deviations in surface smoothness from classes such as road, roof, and ground would make all the difference here. To address this limitation, *DoGSS-PCL* computes additionally f_mIoU , which specifically targets geometric differences between point clouds of objects.

Our metric reveals a limitation in the synthetic point clouds: There exists a significant deviation in geometry for classes such as **CityFurniture** and **BuldingInstallation**. This is reflected prominently in our metric. *DoGSS-PCL* permits a versatile evaluation of the point clouds, avoiding the complexities of comparing multiple independent measures simultaneously.

Table 6 KPConv class-wise $IoU^{(c)}$ and mIoU evaluated on real-world point cloud with training ratio: **real%-synthetics%**. The column **avg.** states the average $IoU^{(c)}$ for each class. The column **corr** displays the correlation coefficient between the class-wise $IoU^{(c)}$ trends and synthetic data ratio.

	100%-0%	75%-25%	50%-50%	25%-75%	0%-100%	avg.	corr.
RoadSurface	0.93	0.94	0.90	0.92	0.55	0.85	-0.70
GroundSurface	0.73	0.69	0.62	0.66	0.35	0.61	-0.80
CityFurniture	0.51	0.35	0.40	0.23	0.23	0.34	-0.90
Vehicle	0.67	0.66	0.51	0.48	0.00	0.46	-0.90
Pedestrian	0.00	0.00	0.00	0.00	0.00	0.00	-
WallSurface	0.71	0.69	0.73	0.69	0.62	0.70	-0.70
RoofSurface	0.01	0.44	0.65	0.20	0.66	0.39	0.60
Door	0.04	0.00	0.00	0.00	0.00	0.01	-0.70
Window	0.24	0.24	0.30	0.17	0.21	0.23	-0.40
BuildingInstallation	0.80	0.11	0.10	0.08	0.13	0.24	-0.70
SolitaryVegetationObject	0.89	0.45	0.88	0.85	0.44	0.70	-0.30
mIoU	0.45	0.45	0.46	0.39	0.29	0.41	-0.80

Table 7 PointNet++ class-wise $IoU^{(c)}$ and mIoU evaluated on real-world point cloud with training ratio: **real%-synthetics%**

	100%-0%	75%-25%	50%-50%	25%-75%	0%-100%	avg.	corr.
RoadSurface	0.64	0.34	0.37	0.42	0.26	0.41	-0.76
GroundSurface	0.27	0.13	0.16	0.20	0.16	0.18	-0.48
CityFurniture	0.03	0.00	0.00	0.00	0.01	0.01	-0.50
Vehicle	0.08	0.01	0.00	0.00	0.00	0.02	-0.78
Pedestrian	0.00	0.00	0.00	0.00	0.00	0.00	-
WallSurface	0.34	0.20	0.32	0.25	0.35	0.29	-0.20
RoofSurface	0.00	0.05	0.00	0.01	0.03	0.02	0.12
Door	0.02	0.00	0.02	0.03	0.00	0.02	-0.25
Window	0.09	0.05	0.06	0.07	0.10	0.07	-0.23
BuildingInstallation	0.05	0.00	0.02	0.04	0.01	0.03	-0.39
SolitaryVegetationObject	0.16	0.14	0.08	0.08	0.07	0.11	-0.90
mIoU	0.15	0.08	0.10	0.10	0.09	0.10	-0.62

Table 8 Class-wise $IoU^{(c)}$, where classes **Pedestrian**, **Vehicle** are not taken into account since dynamic objects were not present in the synthetic dataset.

Class	%
RoadSurface (1):	66.01
GroundSurface (2):	34.75
WallSurface (6):	29.31
RoofSurface (7):	12.67
Doors (8):	42.08
Windows (9):	22.53
BuildingInstallations (10):	10.29

In the synthetic data, classes **Window** and **Road** have been simulated quite accurately, corresponding to 40% and 60% $IoU^{(c)}$. Conversely, classes with more elevated geometric variability, such as **GroundSurface** and **Door**, can only achieve approximately 30%. Highly detailed classes such as **BuildingInstallation** scored low $IoU^{(c)}$ with around 10% because **BuildingInstallation**'s geometry was simplified significantly in our model into simple shapes, which has been well-detected

by **DoGSS-PCL**. The details $IoU^{(c)}$ for each class can be found in Table 8.

Overall, synthetic data exhibits good global and semantic alignment with its real-world counterpart. While the synthetic and real-world point clouds are well-aligned globally, there is still room for improvement in modeling fine-grained geometric details, especially with classes **GroundSurface** and **BuldingInstallation**. These geometric discrepancies can significantly impact the performance of downstream models, as we will explore in the following section.

5.2 Stochastic Approach

We discuss the pros and cons of training the model with our synthetic data based on the observations of the segmentation performances on the real-world point cloud test set. As stated previously, we focused mainly on the results of KPConv.

One of the flaws of synthetic data is their lack of distinct features on planar surfaces, which often leads to under-segmentation. This issue was corroborated by

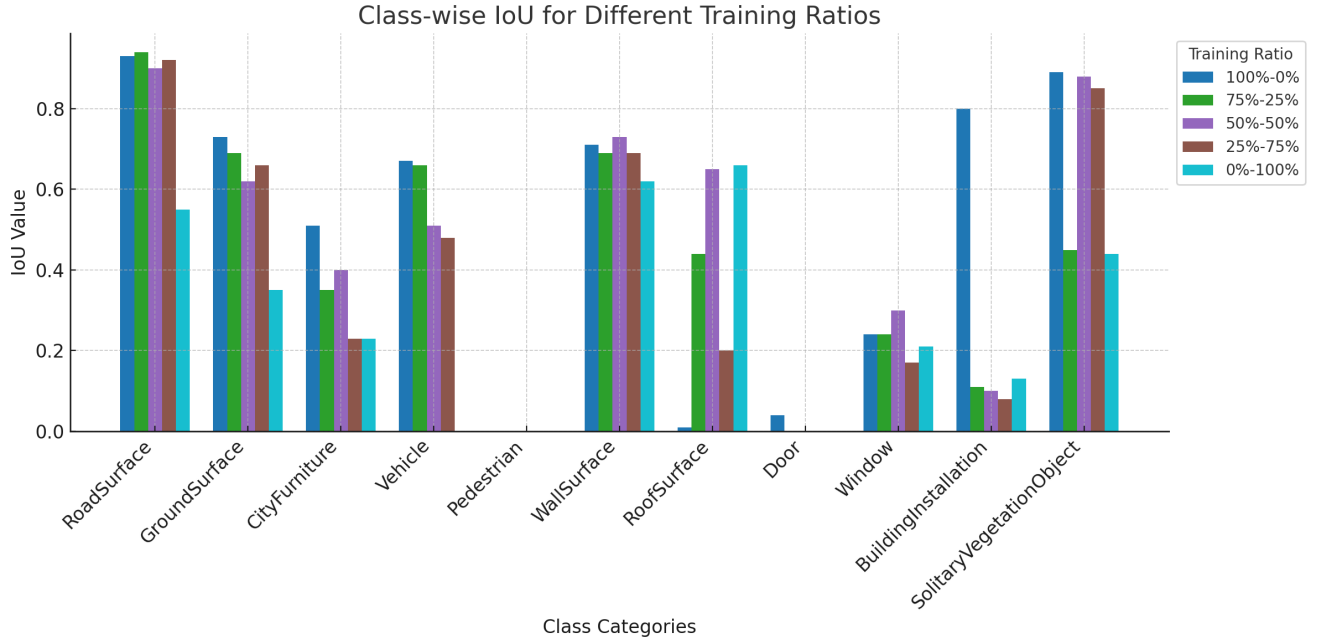


Fig. 13 KPConv results (Table 6) visualized on a bar chart (real vs synthetic). The analysis corroborates the non-linear correlation between the mixed ratio setups with a large dependency on the object in question. The intuitive hypothesis that the performance shall have the highest scores holds for the most classes, with the striking example of **BuildingInstallation** (drop by 70%). Remarkably, for such classes as **Window**, the supplementary synthetic data can increase the generalization capabilities, even outperforming real-only input, presumably due to laser glass-penetration and noise effects rendering real-world point clouds very sparse, in contrast to 3D simulated windows yielding complete windows geometries.

our experiments, as, for example, objects that are geometrically represented by surfaces, such as **RoadSurface** and **GroundSurface** objects, performed gradually worse with the increase of synthetic data, with correlation coefficients of -0.7 and -0.8 , respectively.

Moreover, from Table 9, we observe that **RoadSurface** and **GroundSurface** objects are most easily misclassified and confused with each other owing to limited distinct features. In the real world, instead of flat surfaces without any spectral information, **RoadSurface** and **GroundSurface** objects contain additional low-level (e.g., distinct edge color) and high-level (e.g., spatial relation to other urban elements) features, allowing humans and classifiers to distinguish between them. In synthetic data, these significant features disappear, simplifying both classes into flat, neighboring surfaces, rendering them prone to misclassification. Potentially, such effects can be mitigated by adjusting neural networks' receptive fields.

Another drawback of the virtual models we observed was the wide variety of object structures in the **BuildingInstallation** class, leading to model confusion. The objects in the **BuildingInstallation** class often consist of different parts that have a structure similar to those of other classes. In synthetic data, **BuildingInstallation** objects often consist of irregular shapes as well as vertical flat planes that resemble

WallSurface objects, which is the most misclassified class (see Table 9). The model then fails to extract significant and consistent features for the class.

Although surfaces in synthetic data possess problems of lack-of-feature and objects in the **BuildingInstallation** class lack significant structure, some other classes that have unique and consistent structures are, on the other hand, helpful in training. For example, the segmentation of class **SolitaryVegetationObject** performs well with low dependency on the ratio of synthetic data ($corr. = -0.3$), even though the tree is not accurately modeled in synthetic data. This phenomenon can be explained by the unique and consistent structure of **SolitaryVegetationObject** objects that other classes do not possess. Both real-world and synthetic data consistently represent trees as significant, spherical-like structures with a vertical trunk. As this structure barely appears in other classes, the model can recognize it easily without confusion. The identical structure of **SolitaryVegetationObject** class objects is maintained when the ratio of synthetic data accumulates, thereby providing a consistent learning source for the model. Consequently, this consistency translates into a relatively steady performance, a pattern also observable in the **Window** class. Both in real-world and synthetic data, **Window** objects possess unique structures with window frames and glass surfaces fused, as

Table 9 Most misclassified classes. For example, **GroundSurface** appears most frequently among the false positives of **RoadSurface**, with 95% of appearance.

Wrong Prediction	Most Frequent Class	Proportion
RoadSurface	GroundSurface	95%
GroundSurface	RoadSurface	48%
CityFurniture	GroundSurface	32%
Vehicle	CityFurniture	75%
Pedestrian	-	-
WallSurface	Window	44%
RoofSurface	BuildingInstallation	87%
Door	WallSurface	52%
Window	BuildingInstallation	71%
BuildingInstallation	WallSurface	48%
SolitaryVegetationObject	BuildingInstallation	42%

shown in Figure 14. However, in synthetic data, some **Window** objects are simplified into surfaces without window frames (Figure 14), which causes confusion between **WallSurface** objects and **Window** objects (Table 9).



Fig. 14 Window objects simplified into surfaces (right) and Window objects with complex structure (left).

One of the fascinating results is the increase in model performance on the **RoofSurface** class when the ratio of synthetic data increases. From real-world point clouds, the **RoofSurface** objects are usually incomplete or even missing. They typically have very few points and only cover small parts of the entire roof. In synthetic data, with more flexibility in the control of driving route, angle, and height, the **RoofSurface** class data we acquired were more complete and covered relatively large areas of the roofs, as shown in Figure 15. The **RoofSurface** class could serve as a compelling example of how synthetic data can enhance the performance of object segmentation tasks for rarely observed classes in real-world data. By leveraging the high-level geometric structure of synthetic roof surfaces, the models achieved an $IoU^{(c)}$ of 0.65 instead of only 0.01 when using real-world data alone.



Fig. 15 **RoofSurface** objects in real-world data (left) and the point cloud acquired from its synthetic twin (right).

Overall, we observe that the synthetic point clouds simulated from semantic 3D city models provide two advantages to serve as sources for synthetic data: (1) The ability to preserve structures for objects that possess unique shapes, such as objects in classes **SolitaryVegetationObject**, **Window**, and **RoofSurface**. (2) For the parts missing or occluded in the real-world city point cloud, generating synthetic point clouds from their counterparts in the real-city digital models is a low-cost alternative. On the other hand, some classes, lacking significant features, require refinement to provide unique and meaningful information for recognition. In some cases, such as objects geometrically represented by surfaces or objects in the class **Window**, the model could enhance their features by mixing a portion of the real-world data.

6 Limitations

Our method was primarily designed for the off-the-shelf laser scanner sensor parameters, enabling generic testing without the need to follow manufacturer-specific requirements. This trait also may have influenced the domain gap experiments, as it inevitably introduced sensor-to-sensor parameter deviation. Yet, our method

can also be tested on any sensor-specific settings upon providing the manufacturer's details.

We have tested our method on the approximate driving trajectory of the actual MLS measuring campaign, mimicking the right-hand traffic and keeping a center lane. Consequently, the diverging laser-to-object distance may have occurred and impacted the laser scanning patterns and point cloud density. Nevertheless, our approach allows for loading the actual driving trajectory, if available.

By using the to-date largest real-world-based and highly-detailed semantic road space models, including LOD3 data, we ensured a high level of semantic and geometric information in our virtual testbed. Simultaneously, there were still instances that merely approximate the actual shape of objects, such as tree models (e.g., Figure 11). Also, dynamic objects, such as cars and pedestrians, were not present in the datasets. Future work shall investigate creating even more advanced 3D reality-based virtual testbeds.

Even though we have leveraged a large dataset in the city of Ingolstadt with 100M points in our work, scalability remains a concern. This is because certain features from object classes, such as building facades or building installations, exhibit various characteristics that the neural network models struggle to capture with limited instances.

Furthermore, our evaluation methods employed two well-established semantic segmentation models trained on our datasets. However, the extended evaluation may also use the latest state-of-the-art models (Liu et al. 2024; Zeng et al. 2024), such as transformer-based approaches (Zhao et al. 2021a; Wu et al. 2024) and other datasets, that can complement the analysis.

Worth noting is that in our experimental approach, we sample points from the same geographical regions under the introduced splits. Yet, the framework also allows for testing disjoint geographical analysis within the borders of the provided 3D model. Such an approach may open new application: If the point cloud splits are positively validated under the geographically disjoint areas of a small dataset subset (e.g., city district) and target ratios are established, the full-scale 3D model (e.g., whole city) can be used for simulation and only complemented by expensive manual annotations where required. Eventually, this leads to significant process automation and cost reduction.

7 Conclusion and Outlook

In this work, we present a method to measure the domain gap between simulated and real-world point

clouds both deterministically and stochastically by leveraging digital replicas of real cities and real-world point clouds. We also introduce a novel metric, *DoGSS-PCL*, measuring the quality of synthetically generated point clouds, which effectively measures both the semantic and geometric point cloud quality. The introduced analysis shall serve as a blueprint for future works investigating domain gaps in simulated point cloud generation.

Notably, the experiments also corroborate that our method generates simulated semantic point clouds that can complement real-world point clouds. Intuitively, overall best performance is maintained when using only real and manually annotated point clouds. Yet, we show that the 50%-50% fusion of real and simulated point clouds provides comparable segmentation results to solely using real point clouds, as there is only a 1% overall accuracy difference. Interestingly, we also observe that the ratios are non-linear and largely depend on the target class, e.g., drastic decrease (by 70%) for `BuildingInstallation` when adding only even 25% of synthetic point clouds, or slight increase for `Window` when adding 50% of glass-rich synthetic point clouds. By analyzing this trait, we also conclude that highly detailed semantic 3D city models can be used as semantic-rich training sets for developing data-demanding deep learning methods.

Although the presented results are promising, testing sample size implies that caution must be exercised. We plan to extend the acquired dataset for future work with additional 3D models and point clouds representing various architectural styles and traffic scenarios. A comprehensive analysis of other simulation software shall also be undertaken, including HELIOS++, which comprises detailed sensor model specifications. Another aim is to conduct a geographically disjoint analysis of the real-world 3D model to corroborate the method's usefulness as validation for large-scale applications, underscoring its potential to minimize labour-intensive manual annotations and leverage available 3D models.

Declarations

Acknowledgements We would like to thank Florian Hauck for setting up and designing the experiment for PointNet++. Furthermore, we would also like to thank the Munich Data Science Institute (MDSI) and Dr. Ricardo Acevedo Cabra for the TUM Data Innovation Lab, in the context of which the work was carried out.

Funding This work is supported by the German Federal Ministry of Transport and Digital Infrastructure (BMVI) within the *Automated and Connected Driving*

funding program under the Grant No. 01MM20012K (SAVeNoW).

Conflicts of interest/Competing interests All authors declare that they have no competing interests.

Availability of data and material The semantic models are available under <https://github.com/savenow/lod3-road-space-models>.

Code availability The implementation of the methodology is available under <https://github.com/tum-gis/mind-the-domain-gap>.

Authors' contributions Nguyen Duc: Methodology, Software, Validation, Formal analysis, Investigation, Writing - Original Draft. Yan-Ling Lai: Methodology, Software, Validation, Investigation. Patrick Madlindl: Methodology, Software, Validation, Writing - Original Draft. Xinyuan Zhu: Methodology, Software, Validation. Benedikt Schwab: Conceptualization, Writing - Original Draft, Writing - Review & Editing, Visualization, Supervision. Olaf Wysocki: Conceptualization, Writing - Original Draft, Writing - Review & Editing, Supervision. Ludwig Hoegner: Resources, Writing - Review & Editing, Supervision. Thomas H. Kolbe: Resources, Writing - Review & Editing, Supervision.

References

3D Mapping Solutions (2023) MoSES Mobile Mapping Platform. <https://www.3d-mapping.de/ueber-uns/unternehmensbereiche/data-acquisition/unser-vermessungssystem/>, Accessed: 2023-01-30

ASAM (2023) OpenDRIVE v1.8.0. <https://www.asam.net/standards/detail/opendrive/>, Accessed: 2024-02-15

Batur M, Yilmaz O, Ozener H (2020) A case study of deformation measurements of istanbul land walls via terrestrial laser scanning. *IEEE Journal of Selected Topics in Applied Earth Observations and Remote Sensing* 13:6362–6371, DOI 10.1109/JSTARS.2020.3031675

Biljecki F, Stoter J, Ledoux H, Zlatanova S, Çöltekin A (2015) Applications of 3D City Models: State of the Art Review. *ISPRS Int J Geo-Inf* 4(4):2842–2889, DOI <https://doi.org/10.3390/ijgi4042842>

Chen M, Hu Q, Hugues T, Feng A, Hou Y, McCullough K, Soibelman L (2022) STPLS3D: A Large-Scale Synthetic and Real Aerial Photogrammetry 3D Point Cloud Dataset. DOI <https://doi.org/10.48550/arXiv.2203.09065>, 2203.09065

Dai A, Chang AX, Savva M, Halber M, Funkhouser T, Nießner M (2017) ScanNet: Richly-Annotated 3D Reconstructions of Indoor Scenes. In: Proceedings of the 2017 IEEE Conference on Computer Vision and Pattern Recognition (CVPR), Honolulu, HI, USA, pp 2432–2443, DOI <https://doi.org/10.1109/CVPR.2017.261>

Deschaud JE, Duque D, Richa JP, Velasco-Forero S, Martegui B, Goulette F (2021) Paris-CARLA-3D: A Real and Synthetic Outdoor Point Cloud Dataset for Challenging Tasks in 3D Mapping. *Remote Sens* 13(22), DOI <https://doi.org/10.3390/rs13224713>

Dosovitskiy A, Ros G, Codevilla F, Lopez A, Koltun V (2017) CARLA: An open urban driving simulator. In: Levine S, Vanhoucke V, Goldberg K (eds) *Proceedings of the 1st Annual Conference on Robot Learning (CoRL)*, PMLR, vol 78, pp 1–16

Epic Games (2019) Unreal Engine. URL <https://www.unrealengine.com>, Accessed: 2023-07-01

Gao B, Pan Y, Li C, Geng S, Zhao H (2022) Are We Hungry for 3D LiDAR Data for Semantic Segmentation? A Survey of Datasets and Methods. *IEEE Trans Intell Transp Syst* 23(7):6063–6081, DOI <https://doi.org/10.1109/TITS.2021.3076844>

Ge L, Gao J, Ngo H, Li K, Zhang A (2014) On handling negative transfer and imbalanced distributions in multiple source transfer learning. *Statistical Analysis and Data Mining: The ASA Data Science Journal* 7(4):254–271

Girardeau-Montaut D, Roux M, Marc R, Thibault G (2005) Change Detection on Point Cloud Data Acquired with a Ground Laser Scanner. *ISPRS Int Arch Photogramm Remote Sens Spat Inf Sci* 36

Gräfe G (2007) High Precision Kinematic Surveying with Laser Scanners. *J Appl Geod* 1(4):185–199, DOI <https://doi.org/10.1515/jag.2007.021>

Gröger G, Kolbe TH, Nagel C, Häfele KH (2012) OGC City Geography Markup Language CityGML Encoding Standard. Open Geospatial Consortium: Wayland, MA, USA, 2012

Guan H, Liu M (2021) Domain adaptation for medical image analysis: a survey. *IEEE Transactions on Biomedical Engineering* 69(3):1173–1185

Haider A, Pigniczki M, Köhler MH, Fink M, Schardt M, Cichy Y, Zeh T, Haas L, Poguntke T, Jakobi M, Koch AW (2022) Development of High-Fidelity Automotive LiDAR Sensor Model with Standardized Interfaces. *J Sens* 22(19):7556, DOI <https://doi.org/10.3390/s22197556>

Hanke T, Schaermann A, Geiger M, Weiler K, Hirsenkorn N, Rauch A, Schneider SA, Biebel E (2017) Generation and Validation of Virtual Point Cloud Data for Automated Driving Systems. In: *Proceedings of the 2017 IEEE 20th International Conference on Intelligent Transportation Systems (ITSC)*, IEEE, Yokohama, Japan, pp 1–6, DOI <https://doi.org/10.1109/ITSC.2017.8317864>

Hu Q, Yang B, Khalid S, Xiao W, Trigoni N, Markham A (2021) Towards Semantic Segmentation of Urban-Scale 3D Point Clouds: A Dataset, Benchmarks and Challenges. In: *Proceedings of the 2021 IEEE/CVF Conference on Computer Vision and Pattern Recognition (CVPR)*, IEEE Computer Society, Los Alamitos, CA, USA, pp 4977–4987, DOI <https://doi.org/10.1109/CVPR46437.2021.00494>

Huch S, Scalerandi L, Rivera E, Lienkamp M (2023) Quantifying the LiDAR Sim-to-Real Domain Shift: A Detailed Investigation Using Object Detectors and Analyzing Point Clouds at Target-Level. *IEEE Trans Intell Veh* DOI <https://doi.org/10.1109/TIV.2023.3251650>

IPG Automotive (2024) CarMaker. <https://www.ipg-automotive.com/en/products-solutions/software/carmaker/>, Accessed: 2024-05-20

Jutzi B, Gross H (2009) Normalization Of LiDAR Intensity Data Based On Range And Surface Incidence Angle. *Int Soc Photogramm Remote Sens* 38

Kolbe TH, Donaubauer A (2021) Semantic 3D City Modeling and BIM. In: Shi W, Goodchild MF, Batty M, Kwan MP, Zhang A (eds) *Urban Informatics*, Springer Singapore, Singapore, pp 609–636, DOI https://doi.org/10.1007/978-981-15-8983-6_34

Kolbe TH, Kutzner T, Smyth CS, Nagel C, Roensdorf C, Heazel C (2021) OGC City Geography Markup Language (CityGML) Version 3.0 Part 1: Conceptual Model Standard. Open Geospatial Consortium

Kutzner T, Smyth C, Nagel C, Coors V, Vinasco-Alvarez D, Ishimaru N, Yao Z, Heazel C, Kolbe TH (2023) OGC City Geography Markup Language (CityGML) Version 3.0 Part 2: GML Encoding Standard. Open Geospatial Consortium

Lague D, Brodu N, Leroux J (2013) Accurate 3D Comparison of Complex Topography with Terrestrial Laser Scanner: Application to the Rangitikei Canyon (N-Z). *ISPRS J Photogramm Remote Sens* 82:10–26, DOI <https://doi.org/10.1016/j.isprsjprs.2013.04.009>

Li R, Li X, Heng PA, Fu CW (2020) Pointaugment: An auto-augmentation framework for point cloud classification. In: Proceedings of the 2020 IEEE/CVF Conference on Computer Vision and Pattern Recognition (CVPR), Seattle, WA, USA, DOI <https://doi.org/10.1109/CVPR42600.2020.00641>

Lin Y, Vosselman G, Yang MY (2022) Weakly supervised semantic segmentation of airborne laser scanning point clouds. *ISPRS journal of photogrammetry and remote sensing* 187:79–100

Liu J, Yu R, Wang Y, Zheng Y, Deng T, Ye W, Wang H (2024) Point mamba: A novel point cloud backbone based on state space model with octree-based ordering strategy. *arXiv preprint arXiv:240306467*

Magosi ZF, Li H, Rosenberger P, Wan L, Eichberger A (2022) A survey on modelling of automotive radar sensors for virtual test and validation of automated driving. *Sensors* 22(15):5693, DOI [10.3390/s22155693](https://doi.org/10.3390/s22155693)

Mathworks (2018) RoadRunner. <https://mathworks.com/products/roadrunner.html>, Accessed: 2023-07-01

Matrone F, Lingua A, Pierdicca R, Malinvernì ES, Paolanti M, Grilli E, Remondino F, Murtyoso A, Landes T (2020) A Benchmark for Large-Scale Heritage Point Cloud Semantic Segmentation. *Int Arch Photogramm Remote Sens Spatial Inf Sci XLIII-B2-2020:1419–1426*, DOI <https://doi.org/10.5194/isprs-archives-XLIII-B2-2020-1419-2020>

Mohri M (2018) Foundations of machine learning

Phong BT (1975) Illumination for Computer Generated Pictures. *Commun ACM* 18(6):311–317, DOI <https://doi.org/10.1145/360825.360839>

Qi CR, Yi L, Su H, Guibas LJ (2017) PointNet++: Deep Hierarchical Feature Learning on Point Sets in a Metric Space. In: Proceedings of the 31st International Conference on Neural Information Processing Systems (NeurIPS), Curran Associates Inc., Red Hook, NY, USA, p 5105–5114, DOI <https://doi.org/10.5555/3295222.3295263>

Qian Z, Davis R, van der Schaar M (2024) Synthcity: a benchmark framework for diverse use cases of tabular synthetic data. In: Proceedings of the 37th International Conference on Neural Information Processing Systems (NeurIPS), Curran Associates Inc., Red Hook, NY, USA, DOI <https://doi.org/10.5555/3666122.3666262>

Richa JP, Deschaud JE, Goulette F, Dalmasso N (2022) AdaSplats: Adaptive Splatting of Point Clouds for Accurate 3D Modeling and Real-Time High-Fidelity LiDAR Simulation. *Remote Sens* 14(24), DOI <https://doi.org/10.3390/rs14246262>

Ros G, Sellart L, Materzynska J, Vazquez D, Lopez AM (2016) The Synthia Dataset: A Large Collection of Synthetic Images for Semantic Segmentation of Urban Scenes. In: Proceedings of the 2016 IEEE Conference on Computer Vision and Pattern Recognition (CVPR), pp 3234–3243, DOI <https://doi.org/10.1109/CVPR.2016.352>

Rosenberger P, Holder MF, Cianciaruso N, Aust P, Tamm-Morschel JF, Linnhoff C, Winner H (2020) Sequential LiDAR Sensor System Simulation: A Modular Approach for Simulation-Based Safety Validation of Automated Driving. *Int J Automot Engine Technol* 5(3-4):187–197, DOI <https://doi.org/10.1007/s41104-020-00066-x>

Schwab B, Kolbe TH (2019) Requirement analysis of 3d road space models for automated driving. *ISPRS Ann Photogramm Remote Sens Spatial Inf Sci IV-4/W8:99–106*, DOI [10.5194/isprs-annals-IV-4-W8-99-2019](https://doi.org/10.5194/isprs-annals-IV-4-W8-99-2019)

Schwab B, Beil C, Kolbe TH (2020) Spatio-Semantic Road Space Modeling for Vehicle–Pedestrian Simulation to Test Automated Driving Systems. *Sustain* 12(9), DOI <https://doi.org/10.3390/su12093799>

Shen S, Xia Y, Eich A, Xu Y, Yang B, Stilla U (2023) SegTrans: Semantic Segmentation With Transfer Learning for MLS Point Clouds. *IEEE Geosci Remote Sens Lett* 20:1–5, DOI <https://doi.org/10.1109/LGRS.2023.3294748>

Spiegel S, Chen J (2021) Using Simulation Data From Gaming Environments For Training a Deep Learning Algorithm on 3D Point Clouds. *ISPRS Ann Photogramm Remote Sens Spatial Inf Sci VIII-4/W2-2021:67–74*, DOI <https://doi.org/10.5194/isprs-annals-VIII-4-W2-2021-67-2021>

Stocco A, Pulfer B, Tonella P (2023) Mind the Gap! A Study on the Transferability of Virtual Versus Physical-World Testing of Autonomous Driving Systems. *IEEE Trans Softw Eng* 49(4):1928–1940, DOI <https://doi.org/10.1109/tse.2022.3202311>

Thomas H, Qi CR, Deschaud JE, Marcotegui B, Goulette F, Guibas L (2019) KPConv: Flexible and Deformable Convolution for Point Clouds. In: Proceedings of the 2019 IEEE/CVF International Conference on Computer Vision (ICCV), Seoul, Korea (South), pp 6410–6419, DOI <https://doi.org/10.1109/ICCV.2019.00651>

Vector Informatik (2024) DYN4 - Virtual Test Driving. <https://www.vector.com/dyna4>, Accessed: 2024-05-22

von Neumann-Cosel K (2014) Virtual Test Drive. PhD thesis, Technical University of Munich, Department of Informatics, Munich, Germany

Wang J, Liu Y, Tan H, Zhang M (2024) A survey on weakly supervised 3d point cloud semantic segmentation. *IET Computer Vision* 18(3):329–342

Wang Z, Dai Z, Póczos B, Carbonell J (2019) Characterizing and avoiding negative transfer. In: Proceedings of the IEEE/CVF conference on computer vision and pattern recognition, pp 11293–11302

Winiwarter L, Esmorís Pena AM, Weiser H, Anders K, Martínez Sánchez J, Searle M, Höfle B (2022) Virtual Laser Scanning with HELIOS++: A Novel Take on Ray Tracing-Based Simulation of Topographic Full-Waveform 3D Laser Scanning. *Remote Sens Environ* 269:112772, DOI <https://doi.org/10.1016/j.rse.2021.112772>

Wu C, Bi X, Pfrommer J, Cebulla A, Mangold S, Beyerer J (2023) Sim2real transfer learning for point cloud segmentation: An industrial application case on autonomous disassembly. In: Proceedings of the 2023 IEEE/CVF Winter

Conference on Applications of Computer Vision (WACV), Waikoloa, HI, USA, pp 4520–4529, DOI <https://doi.org/10.1109/WACV56688.2023.00451>

Wu X, Jiang L, Wang PS, Liu Z, Liu X, Qiao Y, Ouyang W, He T, Zhao H (2024) Point transformer v3: Simpler faster stronger. In: Proceedings of the IEEE/CVF Conference on Computer Vision and Pattern Recognition, pp 4840–4851

Wysocki O, Hoegner L, Stilla U (2022) TUM-FAÇADE: Reviewing and Enriching Point Cloud Benchmarks for Façade Segmentation. *Int Arch Photogramm Remote Sens Spatial Inf Sci XLVI-2/W1-2022:529–536*, DOI <https://doi.org/10.5194/isprs-archives-XLVI-2-W1-2022-529-2022>

Wysocki O, Xia Y, Wysocki M, Grilli E, Hoegner L, Cremer D, Stilla U (2023) Scan2LoD3: Reconstructing Semantic 3D Building Models at LoD3 Using Ray Casting and Bayesian Networks. In: Proceedings of the 2023 IEEE/CVF Conference on Computer Vision and Pattern Recognition Workshops (CVPRW), Vancouver, BC, Canada, pp 6547–6557, DOI <https://doi.org/10.1109/CVPRW59228.2023.00696>

Wysocki O, Schwab B, Beil C, Holst C, Kolbe TH (2024) Reviewing open data semantic 3d city models to develop novel 3d reconstruction methods. *Int Arch Photogramm Remote Sens Spatial Inf Sci XLVIII-4-2024:493–500*, DOI [10.5194/isprs-archives-XLVIII-4-2024-493-2024](https://doi.org/10.5194/isprs-archives-XLVIII-4-2024-493-2024)

Xiao A, Huang J, Guan D, Zhan F, Lu S (2022) Transfer Learning from Synthetic to Real LiDAR Point Cloud for Semantic Segmentation. In: Proceedings of the 2022 Association for the Advancement of Artificial Intelligence Conference on Artificial Intelligence (AAAI), Virginia, USA, vol 36, pp 2795–2803, DOI <https://doi.org/10.1609/aaai.v36i3.20183>

Yue X, Wu B, Seshia SA, Keutzer K, Sangiovanni-Vincentelli AL (2018) A LiDAR Point Cloud Generator: from a Virtual World to Autonomous Driving. In: Proceedings of the 2018 ACM on International Conference on Multimedia Retrieval (ICMR), Association for Computing Machinery, Yokohama, Japan, p 458–464, DOI <https://doi.org/10.1145/3206025.3206080>

Zeng C, Wang W, Nguyen A, Xiao J, Yue Y (2024) Self-supervised learning for point cloud data: A survey. *Expert Systems with Applications* 237:121354

Zhang Z, Girdhar R, Joulin A, Misra I (2021) Self-supervised pretraining of 3d features on any point-cloud. In: Proceedings of the IEEE/CVF International Conference on Computer Vision, pp 10252–10263

Zhao H, Jiang L, Jia J, Torr P, Koltun V (2021a) Point Transformer. In: Proceedings of the 2021 IEEE/CVF International Conference on Computer Vision (ICCV), Montreal, QC, Canada, pp 16239–16248, DOI <https://doi.org/10.1109/ICCV48922.2021.01595>

Zhao J, Li Y, Zhu B, Deng W, Sun B (2021b) Method and Applications of LiDAR Modeling for Virtual Testing of Intelligent Vehicles. *IEEE Trans Intell Transp Syst* 22(5):2990–3000, DOI <https://doi.org/10.1109/TITS.2020.2978438>

Zhu J, Gehring J, Huang R, Borgmann B, Sun Z, Hoegner L, Hebel M, Xu Y, Stilla U (2020) TUM-MLS-2016: An annotated mobile LiDAR dataset of the TUM City Campus for semantic point cloud interpretation in urban areas. *Remote Sensing* 12(11):1875